Decomposition-learning-based Output Tracking to Simultaneous Hysteresis and Dynamics Control: High-speed Large-range Nanopositioning Example

Jiangbo Liu[1], Jingren Wang[2], and Qingze Zou[2]

***Abstract*—In this paper, a decomposition-learning-based output tracking approach is proposed to compensate for both hysteresis and dynamics effects on output tracking of hysteresis systems such as smart actuators. Simultaneous hysteresis and dynamics control (SHDC) is needed to fully exploit smart or intrinsically soft actuators/sensors for high-speed, large-range positioning/tracking. It remains still, however, as a challenge to achieve SHDC with both precision (performance) and robustness in general output tracking (i.e., not restricted to periodic/repeated operations), and without complicity in modeling and controller design and/or online implementation. The proposed approach aims to address these challenge, by utilizing libraries of input-output elements *constructed offline* to *online* decompose the partially-known (i.e., previewed) desired output trajectory, and synthesize the control input. Iterative learning control techniques are used *a priori* to obtain the input elements each tracking the corresponding output elements accurately, and the Preisach modeling of hysteresis is employed to obtain the combination coefficients of the synthesized control input. An experimental implementation to high-speed, large-range nanopositioning using piezoelectric actuator is presented to demonstrate the efficiency and efficacy of the proposed approach in achieving SHDC.**

I. Introduction

Simultaneous hysteresis and dynamics compensation (SHDC) is needed in the control of smart materials or intrinsically soft materials, whose input to output mapping presents both hysteresis and vibrational dynamics characteristics. These actuators/sensors provide unique positioning accuracy and/or motion flexibility and compliance, thereby, becoming enabling tools in emerging areas ranging from nanoscale imaging/manipulation [1] to soft robotics [2]. Full exploitation of these actuators/sensors to meet the needed positioning/tracking, however, demands SHDC. Although various techniques [3] have been proposed for the control of smart actuators, it still remains as a challenge to achieve SHDC with both precision (performance) and robustness in general output tracking (i.e., not restricted to periodic/repeated operations), and without complicity in modeling and controller design and/or online implementation.

Further development is needed to achieve SHDC in various applications, particularly in high-speed, large-range output tracking. Both feedback [4] and feedforward [3] control techniques have been developed for controlling hysteresis systems such as piezoelectric actuators. For example, robust-control techniques [5] have been proposed to exceed conventional PID-feedback whose performance has been largely limited by the low-gain margin of the system. However, the *a priori* knowledge of hysteresis was not explored for improving the control performance, particularly, at high speed. Although model of hysteresis can be utilized through an adaptive control framework [6], [7], the modeling process is rather involved, and the design and implementation of the high-order controller can be complicated. Moreover, the tracking performance of feedback-based techniques is limited by the nonminimum-phase zeros (NMP) of the system. Such a NMP-caused limitation in output tracking has been addressed through the development of the stable-inversion-based feedforward control approach [8]. Similar idea of inverse has also been utilized to account for hysteresis effect, by capturing the hysteresis, for example, via the Preisach model [9] or the Prandtl-Ishlinskii model [10], thereby, arriving at SHDC. The inversion-based feedforward control approach, however, requires a careful and complicated modeling process that is prone to modeling errors, and the feedforward controller obtained can be sensitive to system variations, not efficient in accommodating the usually quasi-static uncertainty/variation in systems like smart actuators. Thus, it is challenging to account for both the hysteresis and the dynamics effects, both effectively and efficiently.

These issues related to NMP-zeros, robustness and complexity can be largely alleviated through the development of iterative learning control (ILC) techniques [11], [12], [13], as the effect of NMP-zeros is avoided as the entire desired trajectory is known a priori, and SHDC can be achieved through iterative learning [11]. Moreover, the variations in hysteresis and/or dynamics—of quasi-static nature—can be accounted for via few iterations with minor to no loss of performance, thereby, avoiding the performance-robustness trade-off. Although superior tracking performance has been demonstrated [12], [14] and applied in various nanopositioning applications [15], [1], the ILC framework is limited to repetitive/periodic operations, with the entire trajectory completely known a priori and repeatedly tracked. Increasingly-demanding control needs in emerging applications such as soft robotics [2], however, require SHDC in non-repetitive, general output tracking with the desired trajectory not completely known or even online generated. Thus, there exist needs to address these limitations of ILC for SHDC of hysteresis systems.

The main contribution of this work is the development of a decomposition-learning-based output tracking (DLOT) technique to achieve SHDC. Built upon the recently-developed almost-superpositioning of Hammerstein systems (ASHS) [16], the proposed approach provides an avenue to exploit and integrate *offline, a priori learning* in general online track-

[1]Mathworks Inc., Boston, MA. [2]Department of Mechanical and Aerospace Engineering, Rutgers, The State University of New Jersey, Piscataway, NJ 08854, USA. Jiangbo Liu was with Zou's group during this work. robin2010.liu@gmail.com, qzzou@soe.rutgers.edu.

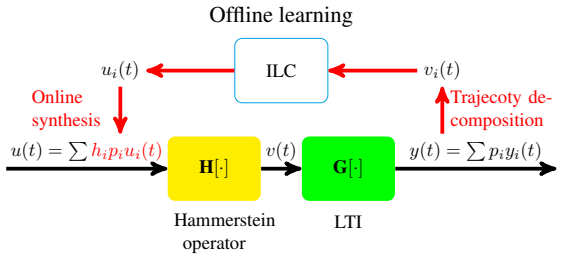

Fig. 1: Schematic illustration of the DLOT technique to hysteresis system consisting of a hysteresis operation $\mathbb{H}[\cdot]$ followed by a linear time invariant dynamics $\Phi(\cdot)$, consisting of off-linear library construction via ILC and online output decomposition and input synthesis.

ing/regulation, by utilizing libraries of input-output elements *constructed offline* to *online* decompose a partially-known (i.e., previewed) desired output trajectory and synthesize the control input, and further enhancing the robustness and performance of the proposed approach through an online adaptation scheme. Particularly, we present the proposed technique in a step-by-step format with practical guidance, followed by an experimental implementation to demonstrate its efficiency and efficacy. The offline learning preserves the advantages of ILC in attaining precision tracking in practical implementation while accounting of quasi-static system variations/changes with little to no loss of tracking precision, and avoiding the NMP-zero effect on tracking performance. Then the library-based decomposition-synthesis mechanism not only achieves SHDC without complexity in modeling, (controller) design and/or implementation, but also lends and extends ILC to general output tracking of hysteresis systems, not limited to repetitive/periodic cases only. Finally, the proposed approach offers efficient online implementation without involving heavy computation. Particularly, the experimental results show that the decomposition-synthesis process to update the control input is only needed at sparse time instants–a rather small fraction (less than 1%) of the total sampling instants of the tracking. Therefore, the proposed approach provides an effective avenue to decouple "training" from "execution" in output tracking, and extends the notion of decomposition and learning [17], [18], [19], [20] from linear systems to hysteresis systems, thereby, pointing to a promising avenue to alleviate the complexities and challenges in modeling and control of hysteresis systems.

II. Decomposition-Learning-based Output Tracking (DLOT) of Hysteresis Systems

Built upon the almost superpositioning principle [16], the key is to achieve SHDC in large-range, high-speed trajectory tracking. We start with capturing the input-output mapping of a hysteresis system, $u(\cdot) \to y(\cdot) : \Re \to \Re$, as a Hammerstein model (see Fig. 1), i.e.,

$$y(t) = \Phi(\mathbb{H}([u(t)])), \quad \text{as in} \tag{1}$$

where $\mathbb{H}[\cdot] : u(t) \to v(t)$, and $\Phi(\cdot) : v(t) \to y(t)$ as in

$$v(t) = \mathbb{H}[u(t)], \quad y(t) = \Phi(v(t)), \tag{2}$$

are the rate-independent nonlinear hysteresis operator and the linear time invariant (LTI) dynamics of the system, respectively, i.e., $\Phi(\cdot)$ is the impulse response of the LTI dynamics. Specifically, we consider that the nonlinear hysteresis operator can be described by a Preisach model, and the desired output trajectory being partially known, i.e., the preview-based output tracking:

Assumption 1. *The inverse mapping of the hysteresis operator $\mathbb{H}[\cdot]$ (from the output to the input) can be described by a Preisach model as*

$$u(t) = \iint_{\alpha \geq \beta} \mu(\alpha, \beta) \gamma_{\alpha\beta}[v(t)] d\alpha d\beta, \tag{3}$$

where α, $\beta \in \Re$, $\mu(\alpha, \beta)$ is the weighting function, and $\gamma_{\alpha\beta}[\cdot]$ is the elemental hysteresis operator, respectively.

Assumption 2. *The desired output trajectory $y_d(t)$ is smooth, and at any given time instant t_c, $y_d(t)$ is known for $t \in [t_c, t_c + T_p]$ and a given preview time $T_p < \infty$.*

The above inverse representation of the hysteresis operator $\mathbb{H}[\cdot]$ as the Preisach model (as in [21]) is to simplify the derivation later, and it can be verified that the Preisach model in Eq. (3) satisfies the following properties:

Proposition 3. *The Preisach model $\mathbb{H}[\cdot]$ is bounded input, bounded output (BIBO) stable and bi-Lipschitz, i.e., for any given continuous input $u(t)$, there exists a constant $L_{\mathbb{H}} \in \Re^+$ such that for any given $t_1, t_2 \in \Re$,*

$$\frac{1}{L_{\mathbb{H}}} |u(t_1) - u(t_2)| \leq |v(t_1) - v(t_2)| \leq L_{\mathbb{H}} |u(t_1) - u(t_2)| . \tag{4}$$

Moreover, the Preisach model $\mathbb{H}[\cdot]$ is nonlinear almost everywhere, i.e., for any given constants $r, c \in \Re$, $m(\{t | \mathbb{H}[u(t)] = r \cdot u(t)\} = 0)$ for any given $u(\cdot) \in \Re$ satisfying $m(\{t | u(t) = c\}) = 0$ ($m(Z)$: the Lebesgue measure of measurable set $Z \subset \Re$), and $v(t) = \mathbb{H}[u(t)] = 0$ if and only if $u(t) = 0$.

As the above Lipschitz constant $L_{\mathbb{H}}$ is range dependent, i.e., $L_{\mathbb{H}}(A_v)$ with A_v the amplitude of the hysteresis output $v(t)$, use of a range dependent $L_{\mathbb{H}}(A_v)$ is preferred over a global constant instead.

The above Proposition implies that the ASHS principle [16] holds in the hysteresis system above, i.e., the response of system (1) to a linear combination of distinct inputs, as the number of the inputs increases, approaches to the linear combination of the responses each corresponding to the respective inputs, provided that the inputs satisfy some smooth conditions (Readers are referred to [16] for the detail). The number of input/output elements required by the almost superposition principle can be quantified [16] by using the *element density*, $\mathbb{D}^*_{\mathbb{H}}$, defined as the number of inputs, $\mathbb{M}^*$ per unit effective length of the trajectory,

$$\mathbb{D}^*_{\mathbb{H}} = \left\lceil \frac{\mathbb{M}^*}{\mathbb{T}_{\mathbb{H}}{}^*} \right\rceil \tag{5}$$

where, respectively, $\lceil \cdot \rceil$ denotes the ceiling function, and $\mathbb{T}_{\mathbb{H}}{}^*$ is the effective trajectory length defined as

$$\mathbb{T}_{\mathbb{H}}{}^* = t^*_{em,f} - t^*_{em,i} \tag{6}$$

with $t^*_{em,f}$ and $t^*_{em,i}$ the time instant of the last and the first local extrema (minima or maxima) of the trajectory to

be decomposed (e.g., the intermediate desired output $v_d(\cdot)$ restricted to the decomposition period).

The central idea of the proposed DLOT technique is to use libraries of input-output elements constructed offline *a priori* to online decompose the previewed desired output and synthesize the control input (see Fig. 1) at some sparse instants only—called the *decomposition instants*. Specifically, the j^{th} decomposition instant, $t_{dec,j}$, is the time at which the previewed desired trajectory $y_d(t)$ within the j^{th} decomposition interval $\mathbf{I}_{d,j}$ is decomposed, i.e.,

$$\begin{aligned} t_{dec,1} &= 0, \quad \text{and for } j > 1 \\ t_{dec,j} &= t_{dec,j-1} + \Delta T_{dec}, \quad \text{with} \\ \Delta T_{dec} &= \mathbf{T}_p - \mathbb{T}^*_{pa}, \quad \text{and} \\ \mathbf{I}_{d,j} &= [t_{dec,j},\ t_{dec,j+1}) \end{aligned} \tag{7}$$

where $\mathbb{T}^*_{pa}$ is the pre-actuation time (quantified a priori, see Step **I**.4 below). In the rest of the paper, we denote the corresponding trajectory considered at the $t_{dec,j}$ instant by using the subscript "j", e.g.,

$$y_{d,j}(t) \triangleq y_d(t), \quad \text{for } t \in \mathbf{I}_{d,j}. \tag{8}$$

To facilitate the implementation, we consider below in the discrete-time domain instead, i.e., $y_{d,j}[i] = \bar{y}_{d,j}(iT_s)$, with all the time intervals (e.g., $\mathbf{I}_{d,j}$) replaced by their discretized counterparts, respectively.

A. DLOT Technique

We present the DLOT technique as an algorithm of four main steps.

1) Step I: Offline Preparation: The *a priori* preparation includes constructing libraries of input-output elements, characterizing the hysteresis curves, and estimating the pre-actuation time and the length of zero-extension (of the previewed desired output—to avoid truncating the elements in the decomposition [17], [18]).

Step I.1: *Construction of Libraries of Input-Output Bases via Iterative Learning.* We propose to construct two libraries, $\mathcal{L}_H$ and $\mathcal{L}_D$, each consisting of pairs of input-output elements for hysteresis and dynamics compensation, respectively. Particularly, each element in libraries $\mathcal{L}_H$ and $\mathcal{L}_D$ will have different amplitude (τ_i) or speed (s_j), respectively,

$$\begin{aligned} \mathcal{L}_H &= \big\{\mathcal{H}_1(\cdot,\tau_1), \mathcal{H}_2(\cdot,\tau_2), \cdots, \mathcal{H}_{N_H}(\cdot,\tau_{N_H})\big\}, \\ \mathcal{L}_D &= \big\{\mathcal{D}_1(\cdot,s_1), \mathcal{D}_2(\cdot,s_2), \cdots, \mathcal{D}_{N_D}(\cdot,s_{N_D})\big\}, \end{aligned} \tag{9}$$

where for each $i = 1, 2, \cdots, N_H$, and $j = 1, 2, \cdots, N_D$, respectively,

$$\mathcal{H}_i = (\ u_{e,i}(\cdot,\tau_i),\ \gamma_{e,i}(\cdot,\tau_i)\ ), \tag{10}$$

are the output element at amplitude τ_i, $\gamma_{e,i}(\cdot,\tau_i)$, and its corresponding input element $u_{e,i}(\cdot,\tau_i)$, respectively, and

$$\mathcal{D}_j = (\ v_{e,j}(\cdot,s_j),\ y_{e,j}(\cdot,s_j)\ ), \tag{11}$$

are the output element at speed s_j, $y_{e,j}(\cdot,s_j)$, and its corresponding input elements, $v_{e,j}(\cdot,s_j)$, respectively. Each amplitude and speed factor, τ_i and s_j, respectively, are within the range of $\tau_i \in [\tau_{\min},\ \tau_{\max}]$ and $s_j \in [s_{\min},\ s_{\max}]$, respectively. The use of elements at different amplitudes and different speeds is for the efficiency in online decomposition/synthesis (in Step **II**)—to accommodate desired outputs over a large amplitude and speed variations. The amplitude and the speed bounds can be easily quantified a priori (based on the tracking requirements and the system characteristics.), and the speed and amplitude factors can be chosen as a trade-off between the offline learning effort and the online control effort, based on the priori knowledge of the desired trajectory and the hardware/effort constraints.

The output elements, $y_{e,j}(\cdot,\tau_i)$s and $\gamma_{e,i}(\cdot,s_j)$s, are generated by using B-spline of chosen order (e.g., 3rd-order B-spline) and amplitude (specified by τ_i), $B(t,\tau_i)$, with

$$B(t,\tau_i) \begin{cases} > 0, & t \in (-p\Psi,\ p\Psi), \\ = 0, & \text{otherwise}, \end{cases} \quad p \in \mathbb{N}, \tag{12}$$

and its time-shifted copies, $B((t-\delta t_k),\tau_i)$ [22], where Ψ is the pre-chosen knot period, and δt_k is the shifting time given by

$$\delta t_k = k\Psi, \quad k \in \mathbb{Z}, \tag{13}$$

respectively. We further define the discretized knot period N_Ψ as

$$N_\Psi \triangleq \lfloor \Psi/T_s \rfloor, \tag{14}$$

with T_s the sampling time.Moreover, it can be easily verified [23] that B-splines are Lipschitz, i.e., there exists a constant $L_v > 0$, such that

$$|B(t_1,\tau_i) - B(t_2,\tau_i)| \le L_v|t_1 - t_2|, \ \text{for } \forall t_1, t_2 \in \Re. \tag{15}$$

The input elements, $u_{e,i}(\cdot)$ and $v_{e,i}(\cdot)$, to track each output elements, $\gamma_{e,i}(\cdot)$ and $y_{e,i}(\cdot)$, correspondingly, are obtained using ILC techniques a priori. To isolate and decouple the hysteresis and dynamics compensation, the speed of the elements in $\mathcal{L}_H$ is kept low so that the vibrational dynamics of the hysteresis system, $\Phi(\cdot)$ in System (1), is not excited when finding the input elements $u_{e,i}(\cdot)$s. Similarly, the amplitude of the elements in $\mathcal{L}_D$ is kept small so that the hysteresis effect, $\mathbb{H}[\cdot]$ in System (1), can be ignored when finding the input elements $v_{e,i}(\cdot)$s in $\mathcal{L}_D$. Then, iterative control techniques such as the inversion-based iterative learning control (IIC) technique [11], [14] can be utilized to compensate for the hysteresis effect or the vibrational dynamics effect, respectively (see Secs. II-A2, II-A3 later). Moreover, the system variations (in hysteresis and/or dynamics) can be easily accounted for without loss of tracking performance by updating the library immediately before the operation—the small size of the libraries renders such an update practically efficient.

Step I.2: *Quantification of the Zero-extension Length* By using the decomposition via redesign-and-extension technique proposed in [23], the previewed desired output (of, in general, non-zero boundary values) can be decomposed with arbitrary precision by using only *one* B-spline and its time-shifted copies. Specifically, at each j^{th} decomposition instant $t_{dec,j}$, the desired output in the first $2pN_\Psi - 1$ sampling period of the decomposition interval, $y_{d,j}(t)$ or $v_{d,j}(t)$ for $t \in [t_{dec,j}, t_{dec,j} + (2pN_\Psi - 1)T_s\ )$, will be redesigned to be smoothly left-transited (i.e., towards $t_{dec,j-1}$) to zero, and then further extended with zeros (see Step **II.1** below). The length of the zero-extension $\mathcal{K}^*_o$ can be quantified based on the required decomposition (approximation) accuracy and the

characteristics of the B-spline (The details are omitted due to space, see Ref.[23]).

Step I.3: *Characterization of the Hysteresis Input-Output Mapping* The values of the Preisach model of the inverse mapping (3) at a sequence of pre-chosen discrete weight values, (α_i, β_j),

$$f(\alpha_i, \beta_j) \triangleq \int_{\beta_j}^{\alpha_i}\int_{\beta_j}^{y} \mu(x,y)\gamma_{xy}[v(t)]dxdy. \qquad (16)$$

are quantified experimentally by applying a sequence of inputs of varying amplitudes (e.g., a triangle wave with ascending and then descending amplitudes) at low speed and measuring the corresponding outputs, where the discrete values of $\alpha_i \in [\alpha_{\min},\ \alpha_{\max}]$ and $\beta_j \in [\beta_{\min},\ \beta_{\max}]$ are chosen based on the range of the output in the given tracking, i.e., the α_is and β_js shall cover the hysteresis mapping appearing in the given output tracking operation, and the discretization-level shall be chosen high enough such that the discretization-caused modeling error can be ignored for the given tracking precision. The obtained sequence of the inverse mapping in Preisach model will be used later to obtain the reference intermediate input $v_d(t)$ for finding the hysteresis-compensating input via decomposition (See Subsec. II-A3 below). Identification of the mapping at discrete weight values (16) is more efficient than identifying the weighting function $\mu(\alpha, \beta)$ itself which is needed in other Preisach-based hysteresis compensation techniques [24].

Step I.4: *Estimation of the Element Density $\mathbb{D}_{\mathbb{H}}{}^*$ and the Preactuation Time $\mathbb{T}^*_{pa}$* The element density $\mathbb{D}^*_{\mathbb{H}}$ can be quantified based on the hysteresis characteristics of system (1) and the previewed desired output (see Eq. (10) in Ref.[16]),

$$\mathbb{D}^*_{\mathbb{H}} = 2\left\lceil \frac{L^*_{\mathbb{H}} L_v}{\epsilon^*_{\mathbb{H}}} \right\rceil \qquad (17)$$

where, respectively, L_v is defined in Eq. (15), $L^*_{\mathbb{H}} = L_{\mathbb{H}}(A_v)$ is the Lipschitz constant (in Eq. (4)) depending on the range of the desired intermediate output A_v, and $\epsilon^*_{\mathbb{H}}$ is the desired tracking precision in terms of the desired intermediate output, i.e., $\|v_{d,j}(t) - v_j(t)\|_{\mathcal{L}_{\infty,T}} \leq \epsilon^*_{\mathbb{H}}$, for $\mathbb{D}_{\mathbb{H},j} \geq \mathbb{D}^*_{\mathbb{H}}$, for $v_{d,j}(t)$, $(t \in \mathbf{I}_{dec,j})$ the previewed desired intermediate output at the j^{th} decomposition instant, and $\mathbb{D}_{\mathbb{H},j}$ the element density used in the j^{th} decomposition instant, respectively.

The preactuation time $\mathbb{T}^*_{pa}$, i.e., the amount of preview of the future desired trajectory needed, can be quantified based on the characteristics of the linear dynamics, $\Phi(\cdot)$, particularly, the non-minimum phase part of $\Phi(\cdot)$. Readers are referred to Ref. [17], [18] for the details.

2) Step II: Online Dynamics Compensation via Superpositioning: The two libraries $\mathcal{L}_H$ and $\mathcal{L}_D$ constructed above will be used online to decompose the previewed desired output at each *decomposition instant* $t_{dec,j}$ $(j = 1, 2, \cdots)$—not at every sampling instant!

Step II.1: *Trajectory Scale-down to Avoid Hysteresis Effect* The previewed desired output $y_{d,j}[\cdot]$ will be first scaled down in amplitude

$$\bar{y}_{d,j}[j] = \lambda_j y_{d,j}[j], \text{ with } \lambda_j \sup_{i\in\mathbf{I}_{d,j}} |y_{d,j}[i]| \leq \mathbf{M}_H \qquad (18)$$

where $\lambda_j \in (0,\ 1)$, and $\mathbf{M}_H \in \Re^+$ is a pre-chosen constant below which the hysteresis effect becomes negligible.

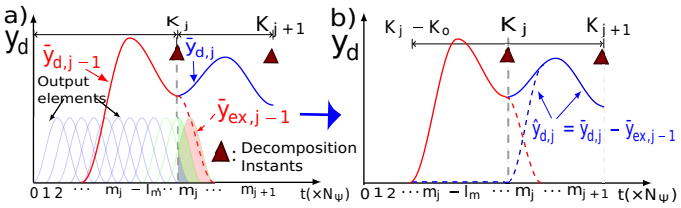

Fig. 2: (a) Extension of the summed weighted output elements (red-dashed curve) for the $(j-1)^{th}$ decomposition interval into the j^{th} one, and (b) the redesign of the desired trajectory in the first $2pN_\Psi - 1$ sampling periods of the j^{th} decomposition interval by using the above extension in (a) (blue-dashed line), and the left-zero-extension.

Step II.2: *Trajectory Redesign to Avoid Truncation in the Decomposition* The decomposition via extension technique will be applied to the scaled-down desired output within each j^{th} decomposition interval. Specifically, we redefine $\hat{y}_{d,j}(t)$ as

$$\hat{y}_{d,j}[i] = \begin{cases} 0, \quad i = K_j - \mathcal{K}_o,\ K_j - \mathcal{K}_o + 1, \ldots,\ K_j - 1; \\ \bar{y}_{d,j}[i] - \bar{y}_{ex,j-1}[i], \\ \quad i = K_j,\ K_j + 1, \ldots,\ K_j + 2pN_\Psi - 1; \\ \bar{y}_{d,j}[i], \\ \quad i = K_j + 2pN_\Psi, \ldots, K_j + \left\lfloor \mathbb{T}^*_{pa}/T_s \right\rfloor. \end{cases} \qquad (19)$$

where $\mathcal{K}_o \geq \mathcal{K}^*_o$ is the zero-extension length as quantified in Step I.2 previously, and $\bar{y}_{ex,j-1}[\cdot]$ is the $(j-1)^{th}$ "tail" trajectory generated from the $(j-1)^{th}$ decomposition—the weighted sum of those output elements employed in the preceding $(j-1)^{th}$ decomposition that enters the current decomposition period $\mathbf{I}_{d,j}$ (see the red-dashed curve in Fig. 2)

$$\bar{y}_{ex,j-1}[i] = \begin{cases} \sum\limits_{k=m_j-p}^{m_j+p} \bar{g}_{k,j-1} y_{e,j}[i - kN_\Psi, s_{j-1}], \\ \quad i = K_j,\ K_j + 1, \ldots, K_j + 2pN_\Psi - 1; \\ 0, \quad \text{otherwise}, \end{cases} \qquad (20)$$

where $\bar{g}_{k,j-1}$s are the coefficients employed in the preceding $(j-1)^{th}$ decomposition, and $y_{e,k}[\cdot, s^*]$s are the output elements in library $\mathcal{L}_D$ at the selected speed s^*, respectively. The above redesigned desired output for the j^{th}-decomposition, $\hat{y}_{d,j}[\cdot]$, now starts at zero with a long enough zero-period (see Fig. 2 (b)) so that the element truncation is avoided with guaranteed decomposition accuracy [23].

Step II.3: *Output Decomposition without Element Truncation* The smoothly-extended trajectory $\hat{y}_{d,j}[\cdot]$ will be decomposed by using the output element at chosen speed s_j in library $\mathcal{L}_D$, $y_e[\cdot, s_j]$, and its time-shifted copies, as

$$\hat{y}_{d,j}[j] \approx \sum_{k=0}^{N_d} \hat{g}_{k,j} y_{e,j}[j - kN_\Psi, s_j] \triangleq \hat{y}_{dd,j}[j], \quad \text{such that,}$$
$$\|\hat{y}_{d,j}[\cdot] - \hat{y}_{dd,j}[\cdot]\|_2 \leq \epsilon_d \qquad (21)$$

where, respectively, $y_{e,k}[j, s_j]$ is as given in Eq. (11), $\epsilon_d \in \Re^+$ is a pre-chosen threshold for the desired approximation accuracy, and the decomposition coefficients, $\hat{g}_{k,j}$s, are obtained via the least square minimization [22], [23].

Then, the decomposition coefficients corresponding to the scaled-down previewed desired output $\bar{y}_{d,j}[\cdot]$ will be obtained via

$$\bar{g}_{k,j} = \begin{cases} \bar{g}_{k,j-1} + \hat{g}_{k,j}, & k = m_j - l_e,\ m_j - l_e + 1, \\ & \ldots,\ m_j + q; \\ \hat{g}_{k,j}, & k = m_j + q + 1,\ m_j + q + 2, \\ & \ldots,\ m_{j+1} + q. \end{cases} \tag{22}$$

where $\bar{g}_{k,j-1}$s and $\hat{g}_{k,j}s$ are given in Eqs. (20) and (21), respectively.

Step II.4: *Intermediate Input (Output) Synthesis via Superpositioning* Finally, the corresponding input (to compensate for the vibrational dynamics) is obtained via the superposition principle as [17]

$$v_{d,j}[i] = \lambda_j \sum_{k=0}^{N_d} g_{k,j} v_{e,j}[i - kN_\Psi, s_j] \tag{23}$$

where λ_j is given by Eq. (18), and $v_{e,k}[\cdot, s_j]$s are the input element at speed s_j in library $\mathcal{L}_D$, $v_e[\cdot, s_j]$, and its time-shifted copies, each corresponding to the output elements $y_{e,k}[\cdot, s_j]$ in Eq. (21), respectively.

3) Step III: Online Hysteresis Compensation via Almost Superpositioning: The input to further compensate for the hysteresis effect will be obtained in the following three steps.

Step III.1 *Intermediate Output Slow-down and Decomposition* To decouple and isolate the hysteresis compensation, the intermediate desired output $v_{d,j}(t)$ is, first, temporally scaled (slowed) down by the speed-factor $\eta_j \in \Re^+$,

$$\bar{v}_{d,j}(t) = v_{d,j}(\frac{t}{\eta_j}), \quad \text{for } i \in \mathbf{I}_{d,j} \tag{24}$$

where the speed factor $\eta_j \geq 1$ is chosen such that the dynamics effect of the hysteresis system is not excited during the tracking of $\bar{v}_{d,j}(t)$. The slowed-down intermediate desired output $\bar{v}_{d,j}(t)$ for $t \in \mathbf{I}_{d,j}$ is then decomposed by using the hysteresis-compensation library $\mathcal{L}_H$, following the same procedure as in Steps **II.1** to **II.3** above,

$$\bar{v}_{d,j}[i] \approx \sum_{k=0}^{N_{h,j}} \bar{g}_{k,j} \gamma_{e,j}[i - kN\Psi, \tau_j],\ i \in \mathbf{I}_{d,j}, \tag{25}$$

where $\gamma_{e,k}[i, \tau_j]$s are the output element at amplitude of τ_j in library $\mathcal{L}_\mathbb{H}$, $\gamma_e[i, \tau_j]$, and its time-shifted copies, and the number of elements N_h is determined by the required element density for hysteresis compensation (see Eq. (17)) as

$$N_{h,j} \geq N^*_{h,j} = \mathbb{D}^*_\mathbb{H} \mathbb{T}_{\mathbb{H},j} \tag{26}$$

where $\mathbb{D}^*_\mathbb{H}$ has been quantified in Step **I.4** (see Eq. (17)), and the effective trajectory length $\mathbb{T}_{\mathbb{H},j}$ is quantified via Eq. (6), respectively.

Step III.2 *Input Synthesis for Hysteresis Compensation* The input to account of the hysteresis effect $\mathbb{H}[\cdot]$ will be obtained as

$$\bar{u}_{d,j}[i] = \sum_{k=0}^{N_h} h_{k,j} \bar{g}_{k,j} u_{e,j}[i - kN_\Psi,\ \tau_j]. \tag{27}$$

where $u_{e,k}[i,\ \tau_j]$s are the input element at amplitude τ_j in library $\mathcal{L}_H$, and its time shifted copies, $\bar{g}_{k,j}$s are as those given in Eq. (25), and $h_{k,j}$s for each $k = 0, \cdots, N_h$ are obtained recursively by

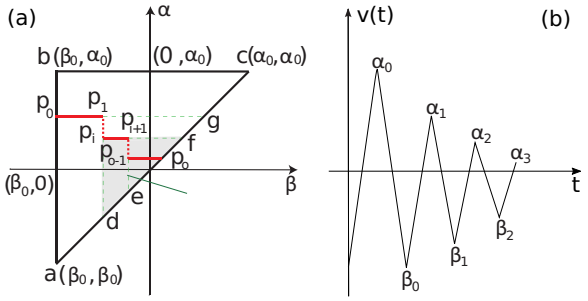

Fig. 3: (a) The Preisach plane and (b) an exemplary output trajectory, where the coordinates of the vertex p_0, p_1, of the stair-case curve, $(\alpha_o,\ \beta_0)$ and $(\alpha_1,\ \beta_1)$, respectively, in (a) correspond to the consecutive local maxima-minima of the output trajectory shown in (b).)

$$\begin{aligned} h_0 &= 1, \\ h_{k,j} &= \frac{1}{\bar{g}_{k,j} G_l} (\bar{u}_d[k] - h_{k-1,j} g_{k-1,j} c_p) \\ &\quad + \sum_{i=2}^{l} \frac{(-1)^{(1+i)} c_p^{i-1}}{\bar{g}_{k,j} \prod_{k=l-i+1}^{l} G_k} \bar{u}_d[k + i - 1], \end{aligned} \tag{28}$$

where $\bar{u}_d[\cdot]$ are the reference input elements obtained by using the Hysteresis input-output mapping obtained in Step **I**.2 (Eq. (16)),

$$\begin{aligned} \bar{u}_d(t) = &-f(\alpha_0, \beta_0) + \\ &2 \left[\sum_{k=1}^{N_m+1} f(\alpha_{p_k - 1}, \beta_{p_{k-1}}) - f(\alpha_{p_k}, \beta_{p_k}) \right], \end{aligned} \tag{29}$$

with $\{\alpha_{p_k},\ \beta_{p_k}\}$ the coordinates of the vertex p_k for $k = 0, 1, \ldots, N_m$ in the Preisach plan (see Fig. 3), where the vertex p_k corresponds to the k^{th} pair of consecutive local maxima and minima of the previewed desired intermediate output $\bar{v}_{d,j}[\cdot]$ as in Eq. (24), i.e., the coordinate of p_i is $(\beta_{p_i},\ \alpha_{p_i})$ when i is odd, and $(\beta_{p_i},\ \alpha_{p_{i+1}})$ when i is even (see Fig. 3 as an example). Moreover,

$$\begin{aligned} c_p &= \frac{u_e[-1]}{u_e[0]}, \text{ and } c_q \triangleq u_e[1]/u_e[0], \\ G_1 &= 1, \quad G_i = 1 - \frac{c_p c_q}{G_{i-1}}, \text{for } i = 2,\ 3, \ldots,\ l, \end{aligned} \tag{30}$$

Step III.3 *Final Input for both Hysteresis and Dynamics Compensation* Finally, the control input to compensate for both hysteresis and dynamics is obtained via temporal scale (speed-up) with the same speed factor η_j,

$$u_{d,j}[i] = \bar{u}_{d,j}\left[\lfloor \eta_j i \rfloor\right], \quad \text{for } i \in \mathbf{I}_{d,j} \tag{31}$$

4) Step IV: Online Adaptation and Optimization: To account for random disturbances and system variations, adaptation factors γ_is are introduced to the decomposition coefficients as,

$$u_{d,j}[i] = \sum_{j=k-1}^{k+2} (h_j \hat{g}_j + \alpha \gamma_j) u_e[i,\ \tau]/\tau, \quad i \in \mathbf{I}_{d,j,k}, \tag{32}$$

where $\mathbf{I}_{d,j,k}$ is the k^{th} decomposition knot period within the j^{th} decomposition period, and Λ^* is the optimal adaptation factor sequence defined as,

$$\mathbf{\Lambda}^* \triangleq [\gamma^*_{k-1},\ \gamma^*_k,\ \gamma^*_{k+1},\ \gamma^*_{k+2}]^T, \tag{33}$$

that minimizes the following cost function of the predicted tracking-error in $\mathcal{L}_2$-norm,

$$\min_{\mathbf{\Lambda}} \sum_{i \in \mathbf{I}_{d,j,k}} (\mathbf{Y}[i]^T \mathbf{\Lambda} - \Omega[i, e[i]])^2, \tag{34}$$

is given by

$$\Lambda^* = \left(\sum_{i \in \mathbf{I}_{d,j,k}} \mathbf{Y}[i]) \mathbf{Y}[i]^T \right)^{-1} \sum_{i \in \mathbf{I}_{d,j,k}} \Omega[t, e[i]] \mathbf{Y}[i]. \tag{35}$$

where

$$\begin{aligned} \mathbf{Y}[i] = & [v_e[i-(k-1)N_\Psi,\ \tau]\ v_e[i-k-N_\Psi,\ \tau] \\ & v_e[i-(k+1)N_\Psi,\ \tau]\ v_e[t-(k+1)N_\Psi,\ \tau]]^T, \end{aligned} \tag{36}$$

$e[i]$ is the tracking error, and $\Omega[i, e[i]]$ is an innovation function to predict the tracking error $e[i]$ for $i \in \mathbf{I}_{d,j,k}$,

$$\Omega[i, e[i]] = e[i - N_\Psi] + \kappa \Omega[i - N_\Psi, e[i - N_\Psi]]. \tag{37}$$

The innovation function $\Omega[i, e[i]]$ is chosen as the inverse of the dynamic part of the system to account for the dynamic effects.

III. High-speed Nanopositioning Experimental Example

We demonstrate the proposed DLOT approach for output tracking by implementing it to the trajectory tracking of a piezoactuator for lateral scanning (x, y direction) on an atomic force microscope (Dimension-ICON, Bruker Nano. Inc.). The first resonant frequency of the piezoactuator was at ∼650 Hz, with full displacement range around 72 μm. The control algorithm was designed and implemented in the MATLAB-xPC-target (Mathworks, Inc.) via a data acquisition system (PCI-6259, National Instrument Inc.).

A. Implementation of the Decomposition-learning-based Output Tracking

1) Offline Preparation (Step I): **Library Construction** The 3^{rd}-order uniform B-spline of 30 seconds duration (slow enough to avoid exciting the dynamics) at 20 different amplitudes were employed as the output elements $\gamma_{e,i}(\cdot, , \tau_i)$ for $i = 1, 2, \cdots, 20$ of the hysteresis-compensation library $\mathcal{L}_H$. The corresponding input elements $u_{e,i}(\cdot, \tau_i)$ ($i = 1, \cdots 20$) were obtained by using the IIC technique [11], as shown in Fig. 4 (a). The maximum of the input elements $\phi(\tau)$ as a function of the amplitude factor τ,

$$\phi(\tau_i) = \sup_t |u_e(t, \tau_i)| \tag{38}$$

was measured directly (see Fig. 4 (b)).

To test the dynamics compensation performance, the 3^{rd}-order B-splines at three different speeds were used as the output elements, $y_{e,i}(\cdot, s_i)$ for $i = 1, 2, 3$, of the dynamics-compensation library $\mathcal{L}_D$. The corresponding input elements, $v_{e,i}(\cdot, s_i)$ ($i = 1, 2, 3$) were also obtained via the IIC technique, and the tracking of one low-speed and one high-speed output element are shown in Fig. 4 (c), (d), respectively, where to test the robustness of the library update, the tracking obtained after over 12 months period (with the same input element) is also compared to those obtained after the update.

Preisach Modeling of the Hysteresis The weighted-integration function $f(\cdot; \cdot)$ of the Preisach model was identified by using a sinusoidal wave with decaying amplitude as the input, after the local memory effect had been removed by driving the piezoactuator to the full range, where a fine-enough discretization level was chosen at 100 (with discretization error $< 0.31\%$ of the total displacement range). The model was validated by comparing the experimentally measured output with the predicted one (under a sinusoidal wave input with a varying amplitude), as shown in Fig. 5(a). The major hysteresis loop presented in Fig. 5 (b) demonstrated that the hysteresis effect was, indeed, pronounced.

Quantification of the Preactuation Time $\mathbb{T}_{pa}$ and the element density D_H^* The preview time for dynamics $\mathbb{T}_{pre}^*$ was quantified as described in [17], and the element density D_H^* was also quantified as described previously, where the decomposition caused approximation error was around the noise level.

B. Online Output Decomposition, Input Synthesis and Optimization (Steps II-IV)

To demonstrate the proposed approach for simultaneous hysteresis-dynamics control, a trajectory with peak-to-peak amplitude of 67.6 μm (94% of the total displacement range) at two different speeds was chosen as the desired trajectory (see Figs. 6, 7). Only a finite preview of the desired trajectory with preview time of T_p = 500, and 20 ms, respectively, was used in the tracking at the low, and high speed, respectively.

In online implementation, first, during each decomposition period, the corresponding portion of the previewed desired trajectory $y_d(t)$ was spatially scaled down by 20 times and then decomposed by using the dynamics compensation library $\mathcal{L}_D$ via linear superposition to obtain the intermediate output decomposition coefficients $\bar{g}_k$s (see Eq. (22))) and the intermediate input $v_d(t)$ (after scaling the signal back);
Secondly, the intermediate output $v_d(t)$ was slowed down by 210, 2625, and 5250 times for the low, medium, and high speed, respectively, and then decomposed by using the hysteresis compensation library $\mathcal{L}_H$. Finally, the compensation factors h_ks was obtained by Eqs. (28) (30), and then online updated via Eqs. (32)- (37), and then combined with the intermediate decomposition coefficients g_ks to obtain the control input.

C. Experimental Results and Discussion

For comparison, tracking by using a well-tuned PI controller and the DC-gain method (where the control input was obtained by simply scaling the desired output by the DC-gain of the system) were also conducted in the experiment, as shown in Figs. 6-7 for the low, medium and high speed, respectively. The comparison of the open-loop to the closed-loop frequency response in Fig. 8 shows that with the PI-controller, the bandwidth of the system was well maintained while the resonant peak was removed. The corresponding relative RMS and relative maximum tracking errors are compared in Table. I. Moreover, we quantified the speed of the desired trajectory by speed ratio λ_s defined

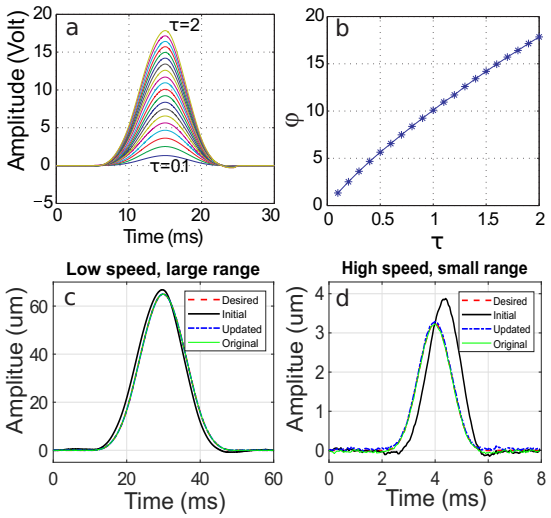

Fig. 4: (a) The input elements for the uniform B-spline based outputs at 20 different amplitudes; (b) The $\varphi(\tau)$ function, and tracking comparison before and after the on-site update for (c) one low-speed element in $\mathcal{L}_H$, and (d) one high-speed element in $\mathcal{L}_D$, respectively.

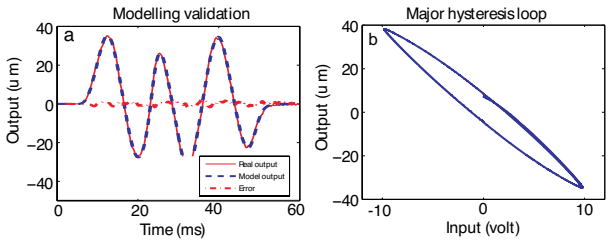

Fig. 5: (a) Validation of the Preisach model of the inverse mapping; (b) The major hysteresis loop of x-axis piezoactuator.

as $\lambda_s = (\sum_{i=1}^{N} \hat{A}_i\omega_i)/\omega_c$, where ω_c is the closed-loop bandwidth, and ω_i and $\hat{A}_i$ are the j^{th} major harmonic frequency component (in the desired trajectory) and its corresponding normalized amplitude, respectively. The speed ratio of the low- and high- speed tracking was at $\lambda_s = 0.0171$ and $\lambda_s = 0.481$ for $N = 6$, respectively.

TABLE I: The relative RMS/Maximum tracking error of the three methods at both low- and high- speed.

	Relative RMS		Relative Maximum	
	Low (%)	High (%)	Low (%)	High (%)
DLOT	1.84	3.96	3.6	5.17
PI	2.12	22.79	5.54	25.3
DC-gain	18.32	26.59	14.4	33.7

The experimental results clearly demonstrated the performance of the proposed method in simultaneous hysteresis-dynamics compensation to achieve accurate tracking, particularly, during high-speed, large-amplitude tracking. At low speed (where the hysteresis effect was pronounced, as manifested by the tracking error of the DC-gain clearly in Fig. 6), the hysteresis effect was almost completely removed by both

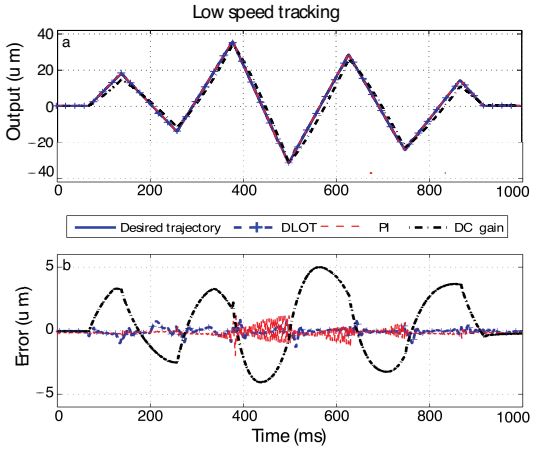

Fig. 6: Comparison of (a) the tracking results by using the proposed DLOT approach to those obtained by using a well-tuned PI controller and the DC-gain method, and (b) the corresponding tracking error for low-speed tracking.

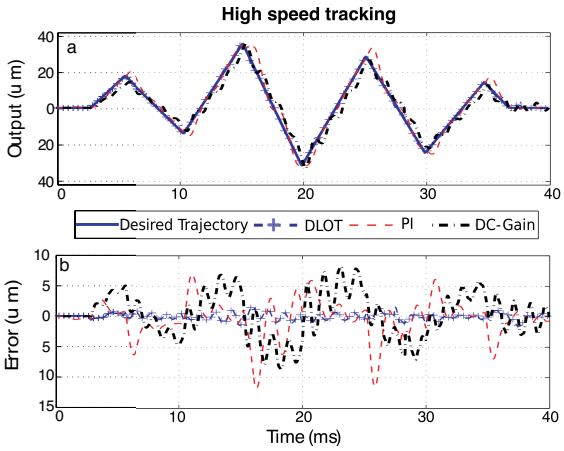

Fig. 7: Performance comparison as in Fig. 6 for high-speed tracking.

the proposed method and the PI feedback. However, in medium and high speed tracking, where both the hysteresis and dynamics effects were expressed, the tracking error of the DC-gain method clearly showed the combined hysteresis-dynamics effects (see Figs. 6, 7). The tracking of the PI-feedback control degraded as the spectrum of the desired output approached to the bandwidth of the closed-loop system, whereas with the proposed technique, a precision tracking with only 3∼4% RMS tracking error was still maintained (see Table 1).

The experimental results also demonstrated the efficacy of the proposed approach in exploiting the benefits of offline learning for robustness and online control efficiency. As shown in Fig. 4 (c), (d), tracking of the elements in the libraries was almost fully restored with a few iterations (∼3 for each output element) despite pronounced tracking error caused by large system (dynamics and hysteresis) behavior changes in a rather long time period (over 12 months). Moreover, only tracking of 23 output elements (at a total of 20 different amplitudes and three different speeds) needed to be learned a priori, and for

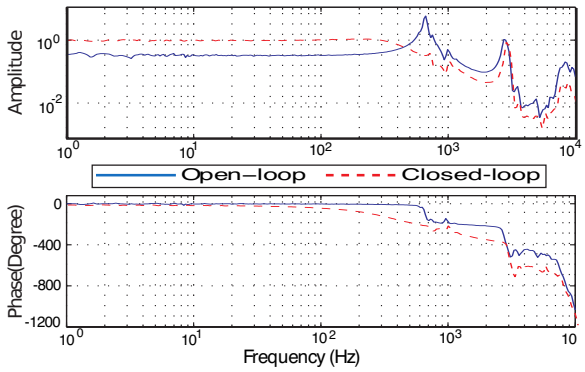

Fig. 8: Bode plot of the x-axis open-loop system vs. that of the closed-loop system with the PI feedback controller used in the experiment.

each decomposition, only 56 elements were needed to meet the element density requirement for hysteresis compensation (see Eq. (17)), and the computation was distributed to a total of less than 5 % of the total number of sampling periods over the entire tracking process. Thus, the online implementation is highly efficient without requiring heavy computations, and by updating the libraries right before the online tracking, the hysteresis and/or dynamics changes be easily accounted for without trading off tracking performance. Therefore, the experimental results also demonstrated the efficacy and efficiency of the proposed technique for control of hysteresis systems.

Conclusion

In this paper, a decomposition-learning-based output tracking approach to achieve simultaneous hysteresis and dynamics control was proposed for non-repetitive operations at high speed and large range. The proposed DLOT technique, presented as a four-step algorithm, consisted of offline construction of libraries of pairs of input-output elements, and online trajectory decomposition and input synthesis, along with temporal and spatial scaling for hysteresis and dynamics separation and decoupling. Experimental implementation on a piezoelectric actuator in high-speed large-range tracking was presented to demonstrate the proposed DLOT technique in compensating for both hysteresis and dynamics effectively and efficiently.

ACKNOWLEDGMENT

This work was supported by NSF grants IDBR-1353890, CMMI-1660355, and CMMI-1851907.

References

[1] J. Ren, Q. Zou, B. Li, and Z. Lin, "High-speed atomic force microscope imaging: Adaptive multiloop mode," *Physical Review E*, vol. 90, no. 1, p. 012405, 2014.

[2] P. Polygerinos, N. Correll, S. A. Morin, B. Mosadegh, C. D. Onal, K. Petersen, M. Cianchetti, M. T. Tolley, and R. F. Shepherd, "Soft robotics: Review of fluid-driven intrinsically soft devices; manufacturing, sensing, control, and applications in human-robot interaction," *Advanced Engineering Materials*, 2017.

[3] G. M. Clayton, S. Tien, K. K. Leang, Q. Zou, and S. Devasia, "A review of feedforward control approaches in nanopositioning for high-speed spm," *ASME Journal of Dynamic Systems, Measurement and Control*, vol. 131, pp. 061101–1 to 061101–19, 2009.

[4] A. Sebastian, A. Gannepalli, and M. Salapaka, "A review of the systems approach to the analysis of dynamic-mode atomic force microscopy," *IEEE Trans. on Control Systems Technology*, vol. 15, no. 5, pp. 952–959, 2007.

[5] C. Lee and S. M. Salapaka, "Robust broadband nanopositioning: fundamental trade-offs, analysis, and design in a two-degree-of-freedom control framework," *Nanotechnology*, vol. 20, no. 3, p. 035501, 2009.

[6] A. Esbrook, X. Tan, and H. K. Khalil, "An indirect adaptive servo-compensator for signals of unknown frequencies with application to nanopositioning," *Automatica*, vol. 49, pp. 2006–2016, 2013.

[7] Z. Li, C.-Y. Su, and X. Chen, "Modeling and inverse adaptive control of asymmetric hysteresis systems with applications to magnetostrictive actuator," *Control Engineering Practice*, vol. 33, pp. 148–160, 2014.

[8] Q. Zou, "Optimalpreview-based stable-inversion for output tracking of nonminimum-phase linear systems," *Automatica*, vol. 45, pp. 230–237, 2009.

[9] Q. Xu and K. K. Tan, "Feedforward control based on inverse hysteresis models," in *Advanced Control of Piezoelectric Micro-/Nano-Positioning Systems*, pp. 23–55, Springer, 2016.

[10] X. Chen, T. Hisayama, and C.-Y. Su, "Adaptive control for uncertain continuous-time systems using implicit inversion of prandtl-ishlinskii hysteresis representation," *Automatic Control, IEEE Transactions on*, vol. 55, no. 10, pp. 2357–2363, 2010.

[11] Y. Wu and Q. Zou, "Iterative control approach to compensate for both the hysteresis and the dynamics effects of piezo actuators," *IEEE Trans. on Control Systems Technology*, vol. 15, pp. 936–944, 2007.

[12] K. Kim and Q. Zou, "A modeling-free inversion-based iterative feedforward control for precision output tracking of linear time-invariant systems," *IEEE/ASME Trans. on Mechatronics*, vol. 18, no. 6, pp. 1767–1777, 2013.

[13] Y. Shan and K. K. Leang, "Accounting for hysteresis in repetitive control design: Nanopositioning example," *Automatica*, vol. 48, no. 8, pp. 1751–1758, 2012.

[14] Z. Wang and Q. Zou, "A modeling-free differential-inversion-based iterative control approach to simultaneous hysteresis-dynamics compensation: High-speed large-range motion tracking example," in *American Control Conference (ACC), 2015*, pp. 3558–3563, IEEE, 2015.

[15] Z. Xu, K. Kim, Q. Zou, and P. Shrotriya, "Broadband measurement of rate-dependent viscoelasticity at nanoscale using scanning probe microscope: Poly(dimethylsiloxane) example," *Applied Physics Letters*, vol. 93, no. 13, p. 133103, 2008.

[16] J. Liu and Q. Zou, "On superposition of hammerstein systems: Application to simultaneous hysteresis-dynamics compensation," *International Journal of Robust and Nonlinear Control*, vol. 28, no. 14, pp. 4075–4092, 2018.

[17] H. Wang, K. Kim, and Q. Zou, "B-spline-decomposition-based output tracking with preview for nonminimum-phase linear systems," *Automatica*, vol. 49, no. 5, pp. 1295–1303, 2013.

[18] H. Wang and Q. Zou, "B-spline-decomposition-based approach to multiaxis trajectory tracking: Nanomanipulation example," *IEEE Trans. Control Systems Technology*, vol. 22, no. 4, pp. 1573–1580, 2014.

[19] S. Devasia, "Iterative machine learning for output tracking," *IEEE Transactions on Control Systems Technology*, 2017. DOI: 10.1109/TCST.2017.2772807.

[20] X. Gao and S. Mishra, "An iterative learning control algorithm for portability between trajectories," in *American Control Conference (ACC), 2014*, pp. 3808–3813, IEEE, 2014.

[21] D. Croft, G. Shedd, and S. Devasia, "Creep, hysteresis, and vibration compensation for piezoactuators: Atomic force microscopy application," *ASME Journal of Dynamic Systems, Measurement and Control*, vol. 123, no. 1, pp. 35–43, March, 2001.

[22] H. Kano, H. Nakata, and C. F. Martin, "Optimal curve fitting and smoothing using normalized uniform b-splines: a tool for studying complex systems," *Applied Mathematics and Computation*, vol. 169, no. 1, pp. 96–128, 2005.

[23] J. Liu and Q. Zou, "On single-basis online asymptotic trajectory decomposition for control applications," in *Advanced Intelligent Mechatronics (AIM), 2016 IEEE International Conference on*, pp. 1291–1296, IEEE, 2016.

[24] Z. Li, C.-Y. Su, and T. Chai, "Compensation of hysteresis nonlinearity in magnetostrictive actuators with inverse multiplicative structure for preisach model," *IEEE Transactions on Automation Science and engineering*, vol. 11, no. 2, pp. 613–619, 2014.